A Multiscale Approach to Axon and Nerve Stimulation Modeling: A Review

M. Stefano, *Member, IEEE*, F. Cordella, *Member, IEEE*, A. Loppini, S. Filippi, and L. Zollo, *Senior Member, IEEE*

***Abstract*— Electrical nerve fiber stimulation is a technique widely used in prosthetics and rehabilitation, and its study from a computational point of view can be a useful instrument to support experimental tests. In the last years, there was an increasing interest in computational modeling of neural cells and numerical simulations on nerve fibers stimulation because of its usefulness in forecasting the effect of electrical current stimuli delivered to tissues through implanted electrodes, in the design of optimal stimulus waveforms based on the specific application (i.e., inducing limb movements, sensory feedback or physiological function restoring), and in the evaluation of the current stimuli properties according to the characteristics of the nerves surrounding tissue. Therefore, a review study on the main modeling and computational frameworks adopted to investigate peripheral nerve stimulation is an important instrument to support and drive future research works. To this aim, this paper deals with mathematical models of neural cells with a detailed description of ion channels and numerical simulations using finite element methods to describe the dynamics of electrical stimulation by implanted electrodes in peripheral nerve fibers. In particular, we evaluate different nerve cell models considering different ion channels present in neurons and provide a guideline on multiscale numerical simulations of electrical nerve fibers stimulation.**

***Index Terms*— Electrical nerve stimulation, axon mathematical model, multiscale simulations, computational model, PNS.**

I. Introduction

ELECTRICAL nerve fiber stimulation is a technique widely used in prosthetics of upper [1] and lower [2] limbs and in therapeutic applications for neural disease treatment [3]. Recently, in the framework of upper limb prosthetics, invasive techniques to electrically stimulate peripheral nerves were used to elicit tactile feedback [4].

In the last years, several neural interfaces were considered for peripheral nerve stimulation studies, among which intraneural interfaces, that can be inserted into the nerve fiber and permit to stimulate fascicles selectively [5]–[7].

In this context, computational models to study electrical nerve fiber stimulation properties represent a useful tool to be used in combination with experiments. In particular, advanced mathematical modeling is needed to achieve greater insights on the biophysical mechanisms driving nerve stimulation, overcoming experimental limitations, like high invasiveness and the in-vivo experiment on animals. Comprehensive models are also necessary for predictions on implant success and can be easily fine-tuned in a personalized medicine framework.

In the literature, some papers deal with electrical nerve fiber stimulation using a computational approach [3], [8]–[11], aiming to forecast the tissues response to the implanted electrode and to evaluate the current stimuli properties considering the tissue characteristics.

To this purpose, detailed microscale neural cell electrical models are combined with macroscale finite element methods (FEM) in a multiscale framework. The modularity of the multiscale description guarantees flexibility concerning the particular stimulating device, the coupling between the macroscale and microscale descriptions, the geometry and type of fibers, up to the ion channels and electrical dynamics of nerves. The resulting computational framework can be used to design and test different types of electrodes, varying geometry, materials, and position of active sites, investigating the electrical dynamics of neural cells when an electrical current is applied.

With these premises, this work aims to in-depth analyse and compare the most used computational models of nerve fibers, paying attention to the animal experimental data used to validate the theoretical model, the myelin sheath presence, and the different type of ion channels considered for each discussed model. Moreover, this paper wants to provide a guideline to develop a multiscale model, which integrates the microscale description of nerves dynamics with macroscale numerical simulations and considers electrodes and volume-conduction in tissues. To the best of our knowledge, there are not review studies in the literature on axon and nerve stimulation modeling based on such multiscale approaches. Therefore, it is expected that this review can give valuable information to

Manuscript received August 27, 2020; revised December 27, 2020; accepted January 15, 2021. Date of publication January 26, 2021; date of current version March 2, 2021. This work was supported in part by the European Union's Horizon 2020 research and innovation programme under Grant 899822 (SOMA project); in part by the INAIL prosthetic center with WiFi Myo-Hand (CUP: E59E19001460005) project; and in part by the Gruppo Nazionale per la Fisica Matematica (GNFM-INdAM). *(Corresponding author: M. Stefano.)*

M. Stefano, F. Cordella, and L. Zollo are with the Research Unit of Advanced Robotics and Human-Centred Technologies, Università Campus Bio-Medico di Roma, 00128 Rome, Italy (e-mail: m.stefano@unicampus.it).

A. Loppini and S. Filippi are with the Research Unit of Nonlinear Physics and Mathematical Modeling, Università Campus Bio-Medico di Roma, 00128 Rome, Italy.

Digital Object Identifier 10.1109/TNSRE.2021.3054551

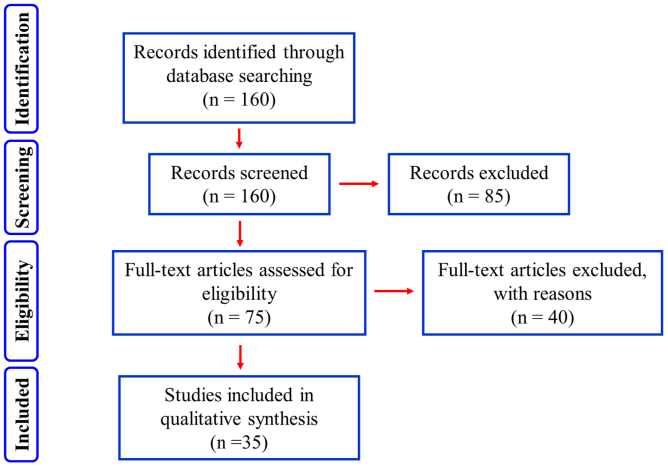

Fig. 1. Flow-diagram of the papers search [13].

the researchers aiming to develop comprehensive simulations on electrical stimulation of peripheral fibers, with important applications in prosthetic [12].

In the following sections, first of all, an overview of the biophysics and ion channel properties of axons, as the different animal models vary, is presented. Secondly, mathematical models of axons considering different arrangements of ion channels according to the corresponding animal model are discussed, giving the reader a perspective on the axons mathematical models used until now. The last section deals with the coupling between neural cell models and FEM-based modeling of fibers stimulation to obtain a multiscale computational framework of the studied case.

Papers were selected from literature with special attention to studies related to computational models of electrical nerve fibers stimulation with application in prosthetic framework, computational models that consider the coupling between mathematical neural cell models and finite element methods simulations, mathematical models of electrical stimulation of neural cell with experimental validation in animals or humans.

Literature research updated to July 2020 was performed using the Google Scholar and PubMed databases. The following keywords were used for the research: *Computational nerve stimulation model*, *Computational axon model*, *ion channels in axons*. All the considered publications were in English language. To select publications relevant to this review aims, the following inclusion criteria were considered: studies related to prosthetics, studies that use electrical nerve fiber stimulation on peripheral nerves, studies on mathematical models of axons. Papers addressing the inclusion criteria were selected. From the initial 160 papers, 85 have been excluded since they did not meet the inclusion criteria. 75 full papers were assessed for eligibility, and 40 papers were excluded since not related to peripheral fibers. A systematic analysis of the remaining 35 papers have been performed (Fig. 1).

II. Ion Channels in Unmyelinated and Myelinated Axons

In this section, ion channels in unmyelinated and myelinated axons are treated in detail. Ion channel expression and distribution in the most investigated animals are considered. Animal species such as mouse, rat, and rabbit are further studied both to account for *in silico* modeling in animals and because of similarities, about neural cells, with humans, i.e., homologous ion channels. Moreover, a large amount of experimental data on animals can be found in the literature to be used for model fine-tuning, parameter optimization, and validation. In the literature, several works studying nerve fibers and neural cells from an experimental point of view, also considering ion channels concentrations changes with respect to spatial location on neurons, are proposed. In particular, a detailed description of anatomical and physiological properties of a generic neural cell, so as of ion channel in mouse, rat, and rabbit nerve fibers is provided. This information will be useful to develop mathematical models of neural cells of the related mammalians.

A. Ion Channel in Mammalian Nerve Fibers

II.A.1): Ion channels in mouse fibers. It is known that there are some resemblances between ion channels in mouse and human. $Na_v1.1$, $Na_v1.2$, $Na_v1.3$ and $Na_v1.7$ channels are encoded by genes that can be found on chromosome 2 in mice and humans, while $Na_v1.5$, $Na_v1.8$ and $Na_v1.9$ are encoded by other type of genes. In PNS cells can be found $Na_v1.8$ and $Na_v1.9$, while $Na_v1.4$ and $Na_v1.6$ can be found in skeletal muscle and in CNS respectively [14]. In the PNS, axons are put in fiber fascicles to form peripheral nerves. The function of peripheral axons is to propagate action potentials to regions far from the body of the cell. Generation and propagation of the action potential happen thanks to voltage-gated (VG) Na^+ and K^+ channels.

In peripheral axons, there are also VG Ca^{2+} channels. *In vitro* studies on mouse sciatic nerves show that if axons are electrically stimulated by pulses, a transient increase in intra-axonal Ca^{2+} concentration occurs along the axons due to the activation of N− and L− type VG calcium channels. So N-type and L-type VG Ca^{2+} channels mediate Ca^{2+} current in peripheral fibers. T-type VG ion channels are calcium channels activated by low voltage. They are present in the C-fibers, i.e. unmyelinated CNS and PNS nerve fibers PNS, and seem to be involved in modulation of action potential conduction velocity [15].

II.A.2:) Ion channel in rat nerve fibers. At juxtaparanodes in normal adult rat sciatic nerve, the K^+ channels $K_v1.1$ and $K_v1.2$ and the cytoplasmic $K_v\beta2$ are observed. Voltage-dependent K^+ channels are not observed in mammalian nodes of Ranvier, as discussed in the following paragraph about rabbit and in reference [16]. These channels can be found in paranodal and internodal regions. In rodents, peripheral nerves at Nodes of Ranvier $K_v7.2$ is observed. It can also be observed in motoneurons in the spinal ventral horn, while $K_v7.3$ is observed in myelinating Schwann cells. $K_v7.2$ and $K_v7.3$ are observed in nodes of small myelinated axons, $K_v7.2$, $K_v7.3$ and $K_v7.5$ are observed in unmyelinated somatic axons, in visceral unmyelinated axons, and in baroreceptor nerve terminals. K_v7 subunits, instead, are observed in peripheral nerves [17].

II.A.3:) Ion channel in rabbit nerve fibers. The first studies on mammalian using voltage-clamp techniques on nerve fibers

were performed on rabbit [16] and rat [18]. From these studies, it was observed that the ionic currents in the rabbit node of Ranvier are a Na^+ current and a leakage current [16]. The Na^+ current is involved in the initial depolarization, and only the leakage current is involved in the repolarization since the K^+ current is not observed.

B. Ion Channels in Humans

In the following section, ion channel properties in human nerve fibers will be treated. From patch-clamp experimental studies on dissociated human axons, several types of VG sodium, VG potassium, and calcium-dependent potassium channels were found [19].

Previous research works pointed out different kinds of VG potassium channels in human peripheral myelinated axons [19], [20], among which: fast (F) channels which rapidly activate and deactivate, with a conductance $\gamma = 50\,\text{pS}$ [19]; slow (S) channels, characterized by slower kinetics, and conductance $\gamma = 10\,\text{pS}$ [20]; intermediate (I) channels, with a time constant intermediate between the values of the other two types of channel cited above, and a conductance $\gamma = 34\,\text{pS}$. In particular, K_v channel α subunits are grouped into 12 different subfamilies (K_v1-12), as observed in the mammalian genome. Among these 12 subfamilies K_v1, K_v3 and K_v7 can be found on axons. Along unmyelinated axons, at Axon Initial Segment (AIS), at juxtaparanodes of myelinated axons and in nerve terminals, $K_v1.1$, $K_v1.2$ and $K_v1\beta2$ can be found [21], [22]. VG calcium channels are involved in a large number of processes, such as the regulation of neurotransmitters release at nerve terminals, excitability, and firing patterns.

Concerning sodium channels, Na_v channels are involved in the initiation and propagation of action potential. Nine different α subunits, $Na_v1.1$-1.9, are encoded by mammalian genes, and, in addition, also auxiliary β subunits can be found. $Na_v1.2$ is observed in a small fraction of nodes of Ranvier in adult myelinated axons. $Na_v1.6$ can be found in both central and peripheral nervous systems. It is known that the Na_v channel α subunits found at the subcellular level is not the same for different types of neurons and different locations in the cell. In myelinated fibers, at the axon initial segment and at the terminal heminodes, $Na_v1.6$ can be found. $Na_v1.3$, $Na_v1.7$, $Na_v1.8$, $Na_v1.9$ can be found in peripheral sensory neural cells [23]–[26].

About calcium channels, T-type calcium channels open subjected to small perturbations from resting potential. In particular, $Ca_v3.2$ T-type channels can be found in central and peripheral neurons as well as in liver, cardiac tissue, and kidney. P/Q-type calcium channels also can be found in mammalian neural cells of PNS and CNS. $Ca_v2.1$ channels can be found at presynaptic terminals of the spinal cord, neuromuscular system, and brain. Calcium N-type channels can be found in CNS and PNS, in particular near synapses, here are involved in the process of the release of neurotransmitters. These ion channels are also involved in the amplification and integration of neural signals [27].

The location of principal ion channels is specified in Table 1 [21], [26]. Finally, it is worth noting that ion channels in human axons show analog features to homologous channels expressed in other mammals or even amphibians, and available data obtained on those species can be used to model axon dynamics in humans.

TABLE I
VOLTAGE-GATED ION CHANNELS

Ion Channel type	Living organism	Location
Sodium channels		
$Na_v1.1$	Human	PNS
$Na_v1.6$	Human, Mouse	PNS
$Na_v1.7$	Mouse	PNS
	Human	Schwann cells
$Na_v1.8$	Mouse, Human	DRG
$Na_v1.9$	Mouse, Human	PNS
Potassium channels		
$K_v1.1$	Human	PNS
$K_v1.2$	Human	PNS
$K_v1.6$	Human	PNS
Calcium channels		
T-type	Human	PNS
P/Q-type	Human	PNS
N-type	Human	PNS

II.B.1): **Ion channels in AIS** The AIS (Fig. 2) has particular electrical properties provided from VG ion channels collected densely [28]. In the AIS we can find:

i) Sodium channels: $Na_v1.1$, $Na_v1.2$ and $Na_v1.6$ isoform of sodium channels can be found in the AIS. $Na_v1.1$ can be found in spinal cord motoneurons [29], in the AIS of retinal ganglion cells [30] and at the AIS of GABAergic neurons [31]. $Na_v1.6$ and $Na_v1.2$ are expressed in the AIS of myelinated and unmyelinated axons. $Na_v1.2$ is involved during development, then it is substituted by $Na_v1.6$ when myelination takes place [32], [33]. $Na_v1.2$ is conserved in the AIS of unmyelinated axons in adult neurons. Notably, Na^+ current density is greater in the AIS of the axon than in the soma [34]. Sodium currents are classified according to biophysical properties: fast inactivating Na^+ current I_{NaT}, the persistent Na^+ current I_{NaP}, and the resurgent Na^+ current [35].

ii) Potassium channels: Potassium channels $K_v1.1$ and $K_v1.2$ can be found in the AIS of inhibitory and excitatory, hippocampal and cortical neural cells, and are positioned more distally than $Na_v1.6$. $K_v2.2$ can be found at the initial segment of medial nucleus trapezoid neurons, while K_v7 channels are in the same region of axons of many central neurons.

iii) Calcium channels: Ca^{2+} channels regulate firing properties. T- and R-type VG Ca^{2+} channels can be found in the initial segment of Purkinje cells and neocortical pyramidal neurons and in the initial segment of brain stem cartwheel cells.

II.B.2:) **Ion channels in axon terminal** The activation of chemical synapses is triggered by the opening of the $Ca_v2.2$ calcium channels and presynaptic $Ca_v2.1$. They can drive signal transmission in the axonal arborization. $Na_v1.2$, $K_v1.1$ and $K_v1.2$ can be observed at axon terminals. K_v3 can be found on excitatory and inhibitory neural cells, while K_v7 is observed on synaptic terminals and preterminal axons.

II.B.3): **Ion channels in unmyelinated axon** $Na_v1.2$ sodium channels support the conduction of action potential.

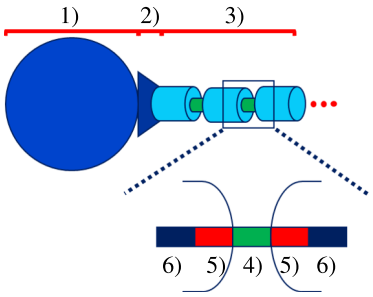

Fig. 2. Scheme of myelinated neuron. 1) Soma; 2) AIS; 3) myelinated axon; 4) node; 5) paranode; 6) juxtaparanode.

In unmyelinated fibers there are more than five voltage gated K^+ channel subunits [36], [37].

II.B.4:) **Channels in the nodes of Ranvier** The signal conduction in myelinated axon is defined saltatory, and it happens thanks to node of Ranvier region, where sodium channels can be found. $Na_v1.1$ and $Na_v1.6$ are the subunits that are on nodes of Ranvier. In the node of Ranvier region, the density of $Na_v1.6$ is greater than the density found in the initial segment [38]. About the sodium currents found on the nodal region, there are persistent and transient macroscopic currents [39], [40]. Conduction along axons can occur thanks to $K_v1.1$, $K_v1.2$ channels in juxtaparanodal region, and $K_v3.1b$, $K_v7.2$ and $K_v7.3$ in the nodal region.

III. Mathematical Models

In this section, the most used mathematical models of neural cells found in the literature will be analyzed. Such models describe the dynamics of membrane potential according to the ion channels observed in the corresponding cells from animals or human experimental data. Membrane voltage is studied to evaluate the activation of nerve fibers when subjected to an external stimulus. These models can be further included in a multiscale simulation by coupling to the stimulating device model, as will be described in the next section. In particular, based on the anatomical nerve fiber reconstruction and finite element methods, the electric potential distribution over the nerve fibers is evaluated given the stimulating electrodes parameters [41]. FEM model results can then be used as input to evaluate nerve fibers activation via the microscale axon biophysical model [42].

A. Computational Neuronal Model

Detailed biophysical neuronal models of axon dynamics represent a fundamental tool for investigating neurons response upon stimulation. They are based on axonal geometry modeling, ion current modeling, and internodal and nodal regions [43], [44]. Some theoretical models, starting from the work of McNeal [45], consider the myelin as a perfect insulator. In literature, the myelin sheath is treated according to three different considerations. The first one models the myelin sheath as a perfect insulator [45], [46], so the dynamics of the model is only defined by the membrane dynamics of the node of Ranvier. This configuration is equivalent to a single-cable electrical circuit model, where the axoplasm

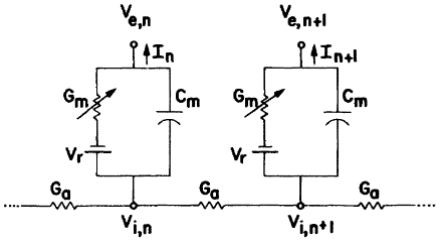

Fig. 3. McNeal equivalent electric circuit scheme, from [45]. G_a is the axial internodal conductance, I_n is the membrane current at node n, $V_{e,n}$ is the external potential at node n, $V_{i,n}$ is the internal potential at node n, G_m is the nodal membrane conductance, C_m is the nodal capacitance, V_r is the resting potential.

is modeled by a single resistor, Fig. 3. Other models treat the myelin sheath as an imperfect insulator [43], [44], [47]. A series of compartments with resistors and capacitors in parallel can model the myelin sheath in a single-cable circuit model. Depending on the research aim, researchers use different types of axon models. The following paragraphs will analyze the most used mathematical axon models: McNeal axon model, SENN model, Sweeney model, mSENN model, MRG model.

B. Voltage-Gated Ion Channels Models

VG ion channels can be modeled by two different methods: Hodgkin-Huxley (HH) or Markov schemes. HH scheme is the most used theoretical model to describe the electrical dynamics of neural cells, but we know that this theoretical model could be limiting in describing the dynamics of ion channels [48]. Markov model approach, in some specific cases, is a better description of the dynamics of ion channels.

According to the HH formalism, the membrane electric potential time change is described by the following equation

$$C_m \frac{dV_m}{dt} = -I_{ion} = -\sum_i I_i \,, \tag{1}$$

where V_m is the membrane potential, C_m is the membrane capacitance, and I_{ion} represents the total transmembrane ion current, driven by different channel types i, also including the leakage channels. Stochastic processes dynamics can be studied by Markov models. They assume that the state of the system at a future time depends only on the current state, i.e., it is a memoryless process. Ion channels, according to the Markov model, are considered as a set of states [49]. Rate constants are defined to explain state transitions and can be related to membrane voltage or not. If we treat a gating variable as a two-state process, a HH model can be turned into a Markov model [50].

1) Neural Cell Models: Every research that proposed an HH model to describe ion channels gating is based on different voltage-clamp studies from amphibians, mammalians, or humans. The work of McIntyre *et al.* [51] used a model that has as a reference experimental voltage-clamp data from myelinated nerve fibers of rabbit sciatic nerve, from [16]. In that model, according to the experimental observations, there are not potassium channels. Kinetic parameters of the HH-type model [52] are different according to the ion channels, and the physiology of the fibers studied. In the

HH scheme, the ion channel current density related to each type of ion is considered. The ionic currents of the model can be written in the form

$$I_i = g_i(V_m - E_i) = \bar{g}_i \prod_j x_j^{p_j} (V_m - E_i) \tag{2}$$

where g_i is the maximum conductance for ion channels i ($\bar{g}_i$) multiplied by one or more gating variables (x_j), depending on activating and inactivating properties. E_i is the reversal potential, and p_j are parameters used to match experimental data. The time evolution of each gating variable is given by

$$\frac{dx}{dt} = \alpha_x(1 - x) - \beta_x x\,, \tag{3}$$

where, for voltage-dependent channels, α_x and β_x are functions of membrane potential and are estimated from experiments. α specifies the transition probability between the closed and the open states, while β is related to the transition between the open and closed states.

Even if with different values of conductance and rate functions, most studies consider potassium and sodium currents, the most common currents found both in amphibian and in mammalian nerve cells. Also, by using HH models, it is possible to consider different ion current contributions, carried by specific channel types (sodium, potassium, or others), by opportunely fine-tuning electrophysiological parameters. In some instances, different types of potassium currents and conductances are considered to describe delayed rectifier K^+ current, slow non-inactivating K^+ current and different type of calcium currents: the high-threshold and low-threshold Ca^{2+} [53]. In several studies, only the difference between fast and slow potassium current is considered.

2) Single Ion Channels: Nowadays, several VG channels are known. In this section, we focus on the ion channels observed in axons: sodium and potassium channels α and β subunits, and N-type, T-type and L-type calcium channels. Some recent papers deal with the modeling of specific ion channels using the HH or Markov scheme. Balbi *et al.* [54] developed a kinetic model representing all α subunits of VG sodium channels. The kinetic model used is a Markov type model. Other studies consider some ion channels treated with the Markov scheme and other ion channels with the HH scheme. For instance, in the work of Feng *et al.* [55], for $Na_v1.6$ and $Na_v1.7$, a Markov type model is used, while an Hodgkin-Huxley type model is considered to model $Na_v1.8$ and $Na_v1.9$. Peters *et al.* [56] employed a HH scheme to describe the $Na_v1.1$ ion channel dynamics. They used the animal model of the Chinese Hamster and considered patch-clamp recordings at different temperatures from ion channels in ovary cells. $Na_v1.2$ and $Na_v1.6$ channels are described by using the HH scheme by Ye *et al.* [57]. In this study, patch-clamp recordings at different temperatures for sodium channels are considered.

The VG potassium channels are encoded by 40 genes. Some potassium channel kinetics and computational models are described by Ranjan *et al.* [58] and are found on Channelpedia [59]. In this framework, both Markov and HH computational models are considered.

VG calcium channels are grouped into three classes: T-type, N-type, and L-type. In the last years, L-type was the only known class: its ion current is also defined as long-lasting calcium current, and it needs a strong depolarization to be activated. N-type currents are only observed in nerves. T-type currents need weak depolarization to be activated and are observed in several cells. Notably, the activation mechanism is almost the same between Na^+ and Ca^{2+} channels [60]. The increase of intracellular concentration of Ca^{2+} ions or of membrane potential can lead to inactivation of L-type Ca^{2+} channels. Faber *et al.* [61] developed a Markov model of the L-type Ca^{2+} channel ($Ca_v1.2$) whose results are compared with experimental data from mammalians. Kinetics of L-type Ca^{2+} is also described by Alekseev *et al.* [62] using patch-clamp studies from ground squirrels.

In summary, all these ion channels models can be considered to build a neuron or axon model choosing the combination of ion channels depending on the physiological properties of the cell to be modeled.

C. McNeal Axon Model

The first model treated in this review is the simplest one: the McNeal axon model. McNeal [45] suggested a model of myelinated nerve fibers considering electrical properties of membranes after a stimulus application that induces the action potential. The McNeal model considers an equivalent circuit to simulate a myelinated nerve fiber (Fig. 3). The approximations are the same as the FitzHugh studies [43], but McNeal considers the myelin sheath as a perfect insulator, fibers infinitely long, nodes of Ranvier regularly spaced, and geometrical properties consistent with the diameters of fibers. The electrical potential outside the fiber is related only to the stimulus current, the electrode geometry, and the tissue surrounding the nerve fiber. It is not affected by the fiber. In this study, a monopolar spherical electrode is considered, located 1 mm away from one node. The current stimuli are monophasic pulses. Fibers are considered of small dimensions to simplify the model and assume that the membranes external surface at all nodes is equipotential. The outer medium with respect to the fibers is considered isotropic and infinite. The membrane voltage dynamics at the node n is described by the equation

$$C_m \frac{dV_n}{dt} + I_{i,n} = G_a(V_{i,n-1} - 2V_{i,n} + V_{i,n+1})\,. \tag{4}$$

The membrane conductance at nodes of Ranvier is constant when stimuli are subthreshold and before the action potential initiation. Only in the node of excitation the membrane dynamics follows the equation of Frankenhauser-Huxley for myelinated frog fibers [63]. The myelinated fiber can be described by the infinite set of linear first-order differential equations, substituting in eq. (4) the ionic current at node n given by $G_m V_n$

$$\frac{dV_n}{dt} = \frac{1}{C_m}[G_a(V_{n-1} - 2V_n + V_{n+1} + V_{e,n-1} - 2V_{e,n} + V_{e,n+1}) - G_m V_n] \quad (n = 0, 1, 2, \ldots, N)\,, \tag{5}$$

where $V_n = V_{i,n} - V_{e,n} - V_r$. $V_{i,n}$ and $V_{e,n}$ are the internal and external potential respectively at node n, G_a and G_m are the axial internodal and the nodal membrane conductances respectively, C_m is the membrane capacitance and V_r is the resting potential. The initial conditions are

$$V_n(0) = 0 \quad \forall n\,. \tag{6}$$

To obtain an approximate solution, it is possible to choose a finite set of differential equations related to the nodes involved and then integrate the set to compute the membrane potentials. The membrane model described in McNeal [45] considers only one node depolarized. At the stimulation node, defined as node 0, if we consider stimulus intensities close to the threshold or greater than it, the ionic current can be defined as

$$I_{i,0} = \pi\, dl(i_{Na} + i_K + i_P + i_L)\,, \tag{7}$$

where d is the axon diameter, l is the nodal gap width, i_{Na}, i_K, i_P, i_L are the ionic currents densities [63]. In this case, the term $G_m V_m$ in eq. (5) is substituted by the term $I_{i,0}$.

D. SENN Computational Axon Model

Reilly *et al.* [64] described another neuroelectric model based on the studies of McNeal. The model included non-linear Frankenhauser-Huxley conductances at each node of Ranvier. This representation is the Spatially Extended Non-linear Node (SENN) model. They studied model results for two types of stimulus waveform: monophasic and biphasic waveform considering human and animal data. The SENN model is a middle ground between a simple single-node model, as the one treated in the previous paragraph, and a more complex node model with myelin representation. The response of the neuron to an extracellular stimulus can be studied by the equivalent electric circuit model. Electrical circuit components made of resistance, voltage source, and trans-membrane capacitance, represent single nodes. The electrical characteristics of the myelin internode are not considered. Membrane conductivity is modeled as reported in the study of Frankenhauser-Huxley [63]. In this study, it is assumed that the current generated from the point electrode is isotropic, and the medium where the electrode is located is uniform. The axon considered has a diameter of 20 μm and internodal spacing of 2 mm. These geometrical properties, the medium, and fibers properties are assigned according to the work of McNeal [45]. The neuroelectric model permits the study of neural dynamics in response to different stimulus parameters, such as polarity, waveshape, and geometric properties related to the neural cell. In this way, the computational model can be used to forecast or guide experiments.

E. Sweeney Axon Model

Another compartmental cable model related to properties of mammalian myelinated fibers of peripheral nerves was developed by Sweeney *et al.* [46]. The model was built considering voltage-clamps studies on rabbit nodes of Ranvier. Also in this work, the nodes of Ranvier are represented by nodal capacitance and voltage-dependent ion channels Na^+ and leakage. As reported in the section II.A.3 about ion channels in rabbit nerve fibers, in the Sweeney *et al.* work, potassium ion channels are not considered. In their model, some similarities with the McNeal model are present: myelin sheath is considered as a perfect insulator. The cable is modeled with 19 compartments, a good choice to study conduction and excitation neglecting interference from the cable end (boundary conditions). Parameters are obtained from the literature, and temperature feedback is introduced via the Arrhenius factor. A rectangular current intracellular stimulus at the center node of Ranvier of a 10 μm diameter fiber model is considered to study properties of excitation. The electric potential time variation at a node is defined as

$$C_m \frac{dE_{m,n}}{dt} + I_{i,n} + \frac{1}{r_a} \times (E_{m,n-1} - 2E_{m,n} + E_{m,n+1}) + I_{inj,n} = 0\,, \tag{8}$$

where C_m is the nodal capacitance, $E_{m,n}$ is the membrane potential at node n, $I_{i,n}$ is the total ionic current at node n, r_a is the internodal axoplasmic resistance, and $I_{inj,n}$ is the intracellular injected current at node n.

F. mSENN Axon Model

The two computational models analyzed above are used to describe the behavior of mammalian nerve fibers [65], [66]. Frijns *et al.* [67] developed a modified SENN model (mSENN) where the changes are in accordance with mammalian nerve fiber data found in literature, also considering the effect of temperature on nerve kinetics. Neurophysiological studies stated that the behavior of nerve fibers is related to temperature [68]: impulse conduction velocity, excitability, action potential amplitude, action potential duration in a nerve fiber are significantly affected by temperature. The temperature dependence can be included based on the Arrhenius equation and by multiplying the activation and inactivation rate constants by a factor ϕ defined as follows

$$\phi = Q_{10}^{(T-T_0)/10}\,, \tag{9}$$

where Q_{10} is a parameter fine-tuned to reproduce temperature-dependent variations as observed in experiments. In this study, besides the introduction of temperature dependence, geometrical properties of the nerve fiber were set to describe a motor fiber of 10 μm diameter. Therefore, taking into account the temperature effects and by introducing a realistic nerve morphology, they obtained a good fit between in vivo and simulated action potentials in terms of shape, duration, and conduction velocity. This model predicts the influence of physiological variations of body temperature on different features of the nerve behavior [67].

G. McIntyre-Richardson-Grill (MRG) Axon Model

In this case, there is a more complex representation of an axon, used to have more insight on mechanisms for depolarizing afterpotentials (DAPs) in myelinated axons [69], [70]. Paranodes, nodes, myelin, and internodes were modeled by using the corresponding electric circuit double cable model, where the myelin is considered as an arrangement of

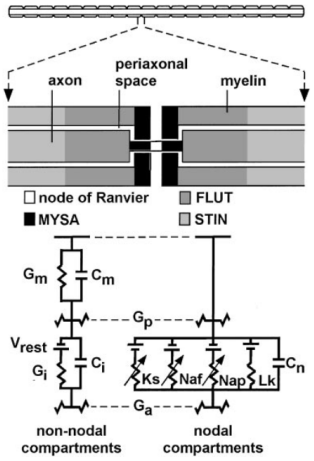

Fig. 4. Double Cable axon model, equivalent electric circuit [77]. In this scheme are expressed myelin conductance and capacitance, G_m and C_m respectively, the rest potential V_{rest}, internodal conductance G_i and capacitance C_i, nodal capacitance C_n and conductances of the ion channels: slow potassium K_s, fast sodium Na_f, persistent sodium Na_p, linear leakage L_k. MYSA, myelin attachment segment; FLUT, paranode main segment; STIN, internode segment.

capacitances and resistors. Studies of Blight [71] and other double-cable models have been used in other works [72]–[75] for reproducing depolarizing afterpotentials.

Other works study how the myelin can affect the conduction and excitation properties of axons to select the better model to describe myelinated axons subjected to extracellular excitation [76]. Several computational models of nerve fibers were considered to describe the propagation of action potentials along the axons for myelinated or unmyelinated fibers. Computational axon models according to the type of nerve cell, including soma, axon, and dendrites, or only axon, have been developed; they may differ depending on whether the cell belongs to the Central or Peripheral Nervous System.

More detailed models of mammalian motor nerve fibers have been developed to deepen the biophysical mechanisms involved in variations of axonal excitability and to control the recovery cycle. A work developed by McIntyre *et al.* [77] studies a double cable axon model, considering nodes of Ranvier, myelin sheath, paranodal and internodal sections Fig. 4. Modeling results are nicely in agreement with experimental data on the excitation properties of mammalian myelinated nerve fibers. All the sets of ion channels at the node and the geometry of the paranode, internode, and myelin were needed to make more accurate the model description to the experimental data. The objectives of the study are related to the influence of afterpotentials on the recovery cycle, but it is interesting noting the properties of the double cable axon model. The geometry and membrane dynamics of the models were based on experimental measurements from human, cat and rat. In this study, 10 segments between two consecutive nodes of Ranvier are used, and myelin attachment segment (MYSA), paranode main segment (FLUT), and internode segment (STIN) regions of the fiber are introduced. By varying the fiber diameters from 5.7 to 16.0 μm, nine models were produced based on experimental measurements of the morphology.

The electrical response of the axons was reproduced by using models based on both linear and nonlinear formulations for membrane voltage dynamics. To describe the dynamics of Nodes of Ranvier are considered nonlinear and persistent sodium conductances, potassium conductance, a leakage conductance, and the membrane capacitance. Previous experimental research studies [19], [20], [78] are considered to describe the dynamics of the ion channels in nodes of Ranvier. From other research studies, it was observed that slow K^+ channels are in the nodes of the mammalian myelinated axon [19], [20], [79]. The parameters about the kinetics of ion channels are considered to reproduce several experimental studies for different fiber diameters. The same dynamics of Richardson *et al.* [76] was used, with the modification of some parameters related to time constants and conductance density [77]. The accurate representation of fiber geometry and nodal membrane dynamics reproduced different experimental data.

IV. Simulation on Stimulation Techniques

This section presents the current approaches in building a multiscale model by coupling the microscale mathematical description of axons and nerve dynamics to the macroscale modeling of fascicles stimulation. In particular, we discuss the different steps needed to obtain the multiscale model, considering the information presented in previous sections. After a mathematical neuron model has been built, to make a comprehensive model that describes the behavior of the nerve fiber subjected to an external stimulus, the anatomical properties and the interaction between tissues and stimuli have to be considered. The first step is to consider mammalian neural cells to model. In this way, it is possible to find the corresponding ion channels expressed in that cells, as treated in Section II. Once the ion channels set to be included in the model is identified, it is possible to choose the preferred mathematical approach for ion currents dynamics and channel kinetics. Also, it has to be evaluated the axon model to adopt, based on the configuration of nodes, myelin sheath, and channel distributions. Notably, all axon models discussed previously can be generalized and personalized to include additional ion current components from different channels. For instance, the MRG axon model treated in Section III could be considered, but if it needs different ion channels, not considered in the MRG model, but observed from the experimental data about the mammalian, the new ion channels can be opportunely modeled and included in the current balance equation.

Concerning the macroscale modeling of the stimulation, several studies in the last years focused on FEM modeling to study the behavior of nerve fibers subjected to electrical stimuli from implanted electrodes [3], [8], [11], [80], [81]. In those investigations, numerical simulations are used to evaluate the electric potential distribution across the nerve fiber. Other studies use the same approach for different stimulation techniques, such as Transcutaneous Electrical Nerve Stimulation (TENS) [80], [82].

The Finite Element model can be built starting from histological images of nerves [9], [83], from micro-computed

tomography (μCT) anatomical studies [84] or magnetic resonance imaging (MRI) data of the subject so as to obtain more accurate results [8]. Following this approach, it is possible to have a more realistic model able to describe nerve-electrode interaction and to study properties of different types of electrodes [11], [85]. Therefore, for instance, it would be possible to investigate the interaction between electrodes and fibrotic tissues and evaluate the better solution for long term implants, and the placement of electrodes in the fibers to obtain more selectivity and fiber recruitment [11]. In the simulation environment, different types of electrodes and stimulation parameters can be tested, with the aim to design optimal stimulation strategies based on computed results, also considering the fibers behaviors. The first step of FEM modeling is the definition of the geometry. As aforementioned, the geometrical model can be built from the anatomical image or other types of data (MRI or computed tomography). Hence, using a FEM software, a 3D model of the anatomical components, including nerve fibers and other tissues, can be developed. In addition to the anatomical model, the electrode model has to be considered and developed. The CAD model of the electrode can be done starting from the technical properties of the specific electrode model, according to the aims of the application. For example, if we consider a peripheral nerve stimulation by intraneural electrodes, we can develop the CAD model according to the properties related to dimension and shape. After this step, the material properties can be assigned to different components: electrode and anatomical regions. Tissue properties can be assigned to different anatomical parts, included in the study. The specific material properties found in the literature are assigned at each region of the model to represent different tissue types. In general, considering peripheral nerve fiber, three different tissues are selected: epineurium, perineurium, and endoneurium. The intrafascicular endoneurium has an anisotropic conductivity tensor with a longitudinal value, and a transverse value [9], [83]. The epineurium and perineurium are assumed to be isotropic media. It is assumed that the nerve is surrounded by a homogeneous saline solution. Electrode models can be made using the same approach, modeling different materials and properties related to them. The physics related to the electrical stimulation problem is solved by integrating Maxwell's equations on the detailed domain presented above in a quasi-static approximation framework. This assumption can be made because of the intensity and duration of the stimuli related to nerve stimulation, as studied in [86]. From the finite element study, it is possible to obtain the electric potential and density current distribution in the nerve fiber after that an electric current is applied. Recently, many works used this approach in the field of neuroprosthetics of upper and lower limb [9]–[11]. The electric potential or current data can be extracted from the simulation software and processed using a data analysis software. Subsequently, the electric potential can be used as the external (extracellular) potential for the neuron or axon models, selected among those cited in the previous sections. Based on the simulated fields, specific signals wave-forms can be built to introduce time-varying stimulations in the micro-scale model. The equations to be solved in the FEM model are

$$\nabla \cdot \vec{J} = Q_j \tag{10}$$

$$\vec{J} = \sigma \vec{E} + \vec{J}_e \tag{11}$$

$$\vec{E} = -\nabla V \tag{12}$$

where $\vec{J}$, Q_j, $\vec{E}$, $\vec{J}_e$, and σ are the current density, the current source, the electric field, the external current density, and the conductivity tensor, respectively. Q_j and $\vec{J}_e$ are set to zero everywhere in the model. A Dirichlet boundary condition $V = 0$ is set at the external region of the cylinder with saline solution, thus imposing the reference potential at infinity.

This assumption is justified by the significantly larger radius of such a cylinder with respect to the dimension of the nerve fascicles. Different approaches for implementing the FEM model have been attempted. Macroscale models developed in literature used the FEM simulation software Comsol Multiphysics, but other FEM modeling environments can be considered, such as FEniCS or Ansys [87], [88].

A peripheral nerves simulator (PyPNS) was recently developed in Python by Lubba *et al.* [89]. In this computational model unmyelinated and myelinated fibers are considered. To describe their electrical dynamics the HH model and the MRG axon model were used respectively. The electric potential is extracted from FEM simulations, assigning different tissue properties in a similar way to that treated above, and is imported into the python simulator to study axons activation. In this work the following assumptions are considered: the axon behavior is not dependent on the other fiber close to it; properties related to the type of ion channels and geometry of axons are fixed; quasi-static approximation of Maxwell's equations is applied to the space that surrounds the fibers; the assumption of purely resistive media is considered for all the tissues. As in [89], to reduce computational time, the electric potential is precomputed in the FEM model and imported in PyPNS. The FEM model has specific settings, and is based on a simplified circular symmetric geometry, including axons and epineurium, and the properties of saline solution for the environment surrounding the nerve model are also considered.

There exist works that study not only the electrical stimulation of axons but also other types of peripheral nerves stimulation. A recent work [90] studied magnetic neural stimulation using computational models. To forecast the stimulation thresholds of in vivo magnetic stimulation of rat sciatic nerve and to compute the electric fields induced by the magnetic stimulation, a multiresolution impedance method coupled with the Frankenhauser-Huxley axon model to study the fiber activation according to the related membrane dynamic properties has been produced. The work takes into account the effects of fascicles and axons location and their electrical properties, which play an important role in the predicting of induced electric fields.

V. Discussion

Knowing the type of ion channels that can be found on peripheral nerve fibers is important for researchers working in the framework of computational models of electrical

TABLE II
SUMMARY OF MAIN FEATURES OF THE MATHEMATICAL MODELS

	McNeal	SENN	Sweeney	mSENN	MRG
Equivalent electric circuit	Single cable	Single cable	Single cable	Single cable	Double cable
number of Nodes of Ranvier	11,21,31.	91	19 compartments	10,20,25,60	21
myelin sheath	perfect insulator	perfect insulator	perfect insulator	perfect insulator	explicit representation
dynamics	F-H non linear equations only in the excitation node	F-H non linear equations on all the nodes of Ranvier	Sweeney equations on all the nodes of Ranvier	like SENN	MRG equations on all the nodes of Ranvier
body temperature	20 °C	20 °C	37 °C	37 °C	37 °C
fiber diameter	20μm	20μm	10μm	10μm	9 values from 5.7 to 16 μm
model based on studies of	frog	frog	rabbit	frog	human, rat, cat

nerve stimulation. In fact, according to the animal model and the type of nerve fibers to be studied, specific settings of ion channels can be modeled. In the previous sections, the most used mathematical models of nerve fibers and ion channels membrane potential dynamics in mammalians and humans have been treated. The aforementioned computational models are compared to pave the way for new researches on neuroprosthesis multiscale simulation. Aspects related to computational cost should be considered in both neuronal and FEM modeling. It is evident that the main aspects influencing computational cost, a part the characteristics of the machine used to implement the simulations, are the adopted geometry of the nerves and the temporal resolution of the numerical approximation of equations.

In Section III on mathematical models of axons, two different types of equivalent electric circuits are considered: a single cable model and a double cable model. In all the analyzed mathematical models that used the single cable model, the axons myelin sheath is considered a perfect insulator, so, in the equivalent electric circuit, it is modeled as a high-value resistance. On the other hand, the double cable model used in the MRG work considers an explicit representation of the myelin sheath and also other sections between two consecutive nodes of Ranvier. In particular, internodal and paranodal sections are considered. Hence, it is possible to affirm that according to experimental validation of these studies and the equivalent electric circuit consideration, the MRG model can be more realistic to represent human axons.

Ion channels treated in the original microscale models can be considered, or they can be modified according to the nerve fibers that researchers want to study, also considering other ion channels if needed. The number of nodes of Ranvier and, accordingly, the length of the axon considered in the computational model depend on the boundary condition that has to be set and on the morphology of the real fiber to be studied. In all the models, the condition is that the membrane potential is zero at the boundary. According to the used parameters, the number of nodes can be selected. In the models analyzed, different numbers of nodes are used, as shown in Table II. According to the considered model, the electrical properties of the equivalent circuit of the nodes are different. The computational models used different equations to describe the dynamics in nodes of Ranvier. The MRG model is based on parameters from human, rat, and cat data. It describes mammalian experimental data, so it is the model more suitable for human fibers compared to the other models that are based on amphibian or rabbit (no potassium channels) data.

The fiber diameters considered in the models are in the range from 10 to 20 μm. All these diameters can be considered for human fibers, so the choice of the fiber diameter has to be done according to the anatomical properties to be modeled. The described models are also different in considering the body temperature in the description. Sweeney, mSENN, and MRG models used body temperature of mammalian.

VI. CONCLUSION

In this review, a multiscale approach to neural cell stimulation has been treated. The first part deals with the physiology of neural cells in different animal models, starting from mammals to get to humans. The second part deals with mathematical models of neural cells considered in the literature for describing their behavior. In particular, the elements to be considered to build an axon model are treated, from unmyelinated nerve fiber discarding temperature dependence, up to a double-cable axon model including nodal and internodal sections surrounded by myelin sheet, and temperature feedback. The third part deals with the combination between microscale mathematical models and macroscale FEM models, taking into account anatomical tissues and electrodes features or other devices stimulation properties.

This review can be useful to develop new multiscale studies on neural cell stimulation, taking into account different types of ion channels according to the physiology of nerve cells and to the specific stimulation techniques, with the aim of defining a comprehensive mathematical model for *in silico* experiments. Indeed, such a framework can be easily generalized to include other stimulating techniques, such as focused ultrasound stimulation or transcutaneous electrical nerve stimulation.

In conclusion, the use of computational modeling is a very helpful instrument to study nerve fibers stimulation techniques. Thanks to these models, it is possible to obtain quantitative results about the behavior of the tissues subject to external stimuli, then the results can be used to forecast the experimental outcomes. If needed, it is possible to modify the experimental conditions or otherwise to design stimulation devices according to the simulation results.

REFERENCES

[1] K. H. Polasek, H. A. Hoyen, M. W. Keith, R. F. Kirsch, and D. J. Tyler, "Stimulation stability and selectivity of chronically implanted multicontact nerve cuff electrodes in the human upper extremity," *IEEE Trans. Neural Syst. Rehabil. Eng.*, vol. 17, no. 5, pp. 428–437, Oct. 2009.

[2] L. E. Fisher, D. J. Tyler, J. S. Anderson, and R. J. Triolo, "Chronic stability and selectivity of four-contact spiral nerve-cuff electrodes in stimulating the human femoral nerve," *J. Neural Eng.*, vol. 6, no. 4, Aug. 2009, Art. no. 046010.

[3] E. Salkim, A. Shiraz, and A. Demosthenous, "Effect of model complexity on fiber activation estimates in a wearable neuromodulator for migraine," in *Proc. IEEE Biomed. Circuits Syst. Conf. (BioCAS)*, Oct. 2017, pp. 1–4.

[4] L. Zollo *et al.*, "Restoring tactile sensations via neural interfaces for real-time force-and-slippage closed-loop control of bionic hands," *Sci. Robot.*, vol. 4, no. 27, Feb. 2019, Art. no. eaau9924.

[5] A. Cutrone *et al.*, "A three-dimensional self-opening intraneural peripheral interface (SELINE)," *J. Neural Eng.*, vol. 12, no. 1, Feb. 2015, Art. no. 016016.

[6] C. M. Oddo *et al.*, "Intraneural stimulation elicits discrimination of textural features by artificial fingertip in intact and amputee humans," *eLife*, vol. 5, pp. 1–27, Mar. 2016.

[7] W. Poppendieck *et al.*, "A new generation of double-sided intramuscular electrodes for multi-channel recording and stimulation," in *Proc. 37th Annu. Int. Conf. IEEE Eng. Med. Biol. Soc. (EMBC)*, Aug. 2015, pp. 7135–7138.

[8] A. N. Shiraz, M. Craggs, B. Leaker, and A. Demosthenous, "Minimizing stimulus current in a wearable pudendal nerve stimulator using computational models," *IEEE Trans. Neural Syst. Rehabil. Eng.*, vol. 24, no. 4, pp. 506–515, Apr. 2016.

[9] S. Raspopovic, M. Capogrosso, and S. Micera, "A computational model for the stimulation of rat sciatic nerve using a transverse intrafascicular multichannel electrode," *IEEE Trans. Neural Syst. Rehabil. Eng.*, vol. 19, no. 4, pp. 333–344, Aug. 2011.

[10] M. Zelechowski, G. Valle, and S. Raspopovic, "A computational model to design neural interfaces for lower-limb sensory neuroprostheses," *J. NeuroEng. Rehabil.*, vol. 17, no. 1, pp. 1–13, Dec. 2020.

[11] S. Raspopovic, F. M. Petrini, M. Zelechowski, and G. Valle, "Framework for the development of neuroprostheses: From basic understanding by sciatic and median nerves models to bionic legs and hands," *Proc. IEEE*, vol. 105, no. 1, pp. 34–49, Jan. 2017.

[12] F. Cordella *et al.*, "A force-and-slippage control strategy for a poliarticulated prosthetic hand," in *Proc. IEEE Int. Conf. Robot. Automat. (ICRA)*, May 2016, pp. 3524–3529.

[13] A. Liberati, J. Tetzlaff, D. G. Altman, and The PRISMA Group, "Preferred reporting items for systematic reviews and meta-analyses: The PRISMA statement," *PLoS Med.*, vol. 6, no. 7, 2009, Art. no. e1000097.

[14] F. H. Yu and W. H. Catterall, "Overview of the voltage-gated sodium channel family," *Genome Biol.*, vol. 4, no. 3, p. 207, 2003.

[15] R. Barzan, F. Pfeiffer, and M. Kukley, "N- and L-type voltage-gated calcium channels mediate fast calcium transients in axonal shafts of mouse peripheral nerve," *Frontiers Cellular Neurosci.*, vol. 10, p. 135, Jun. 2016.

[16] S. Y. Chiu, J. M. Ritchie, R. B. Rogart, and D. Stagg, "A quantitative description of membrane currents in rabbit myelinated nerve," *J. Physiol.*, vol. 292, no. 1, pp. 149–166, Jul. 1979.

[17] J. Fleckenstein, R. Sittl, B. Averbeck, P. M. Lang, D. Irnich, and R. W. Carr, "Activation of axonal Kv7 channels in human peripheral nerve by flupirtine but not placebo–therapeutic potential for peripheral neuropathies: Results of a randomised controlled trial," *J. Transl. Med.*, vol. 11, no. 1, p. 34, Dec. 2013.

[18] T. Brismar, "Potential clamp analysis of membrane currents in rat myelinated nerve fibres," *J. Physiol.*, vol. 298, no. 1, pp. 171–184, Jan. 1980.

[19] A. Scholz, G. O. Reid, W. E. Vogel, and H. U. Bostock, "Ion channels in human axons," *J. Neurophysiol.*, vol. 70, no. 3, pp. 1274–1279, 1993.

[20] G. Reid, A. Scholz, H. Bostock, and W. Vogel, "Human axons contain at least five types of voltage-dependent potassium channel," *J. Physiol.*, vol. 518, no. 3, pp. 681–696, Aug. 1999.

[21] M. N. Rasband *et al.*, "Ion channel localization in axons," in *Encyclopedia of Neuroscience*. New York, NY, USA: Academic, 2009, pp. 229–235.

[22] B. Rudy *et al.*, "Voltage gated potassium channels: Structure and function of Kv1 to Kv9 subfamilies," in *Encyclopedia of Neuroscience*. New York, NY, USA: Academic, 2009.

[23] M. D. L. Ruiz and R. L. Kraus, "Voltage-gated sodium channels: Structure, function, pharmacology, and clinical indications," *J. Medicinal Chem.*, vol. 58, no. 18, pp. 7093–7118, Sep. 2015.

[24] A. L. Goldin *et al.*, "Nomenclature of voltage-gated sodium channels," *Neuron*, vol. 28, no. 2, pp. 365–368, 2000.

[25] T. Li and J. Chen, "Voltage-gated sodium channels in drug discovery," in *Ion Channels in Health and Sickness*, F. S. Kaneez, Ed. IntechOpen, 2018.

[26] J. L. Salzer, P. J. Brophy, and E. Peles, "Molecular domains of myelinated axons in the peripheral nervous system," *Glia*, vol. 56, no. 14, pp. 1532–1540, Nov. 2008.

[27] T. P. Snutch, "Voltage gated calcium channels," in *Encyclopedia of Neuroscience*. New York, NY, USA: Academic, 2009.

[28] M. H. P. Kole and G. J. Stuart, "Signal processing in the axon initial segment," *Neuron*, vol. 73, no. 2, pp. 235–247, Jan. 2012.

[29] A. Duflocq, B. Le Bras, E. Bullier, F. Couraud, and M. Davenne, "Nav1.1 is predominantly expressed in nodes of Ranvier and axon initial segments," *Mol. Cellular Neurosci.*, vol. 39, no. 2, pp. 180–192, Oct. 2008.

[30] A. Van Wart, J. S. Trimmer, and G. Matthews, "Polarized distribution of ion channels within microdomains of the axon initial segment," *J. Comparative Neurol.*, vol. 500, no. 2, pp. 339–352, Jan. 2007.

[31] I. Ogiwara *et al.*, "$Na_v1.1$ localizes to axons of parvalbumin-positive inhibitory interneurons: A circuit basis for epileptic seizures in mice carrying an Scn1a gene mutation," *J. Neurosci.*, vol. 27, no. 22, pp. 5903–5914, May 2007.

[32] T. Boiko *et al.*, "Compact myelin dictates the differential targeting of two sodium channel isoforms in the same axon," *Neuron*, vol. 30, no. 1, pp. 91–104, Apr. 2001.

[33] T. Boiko, A. Van Wart, J. H. Caldwell, S. R. Levinson, J. S. Trimmer, and G. Matthews, "Functional specialization of the axon initial segment by isoform-specific sodium channel targeting," *J. Neurosci.*, vol. 23, no. 6, pp. 2306–2313, Mar. 2003.

[34] W. Hu, C. Tian, T. Li, M. Yang, H. Hou, and Y. Shu, "Distinct contributions of $Na_v1.6$ and $Na_v1.2$ in action potential initiation and backpropagation," *Nature Neurosci.*, vol. 12, pp. 996–1002, Jul. 2009.

[35] I. M. Raman and B. P. Bean, "Resurgent sodium current and action potential formation in dissociated cerebellar purkinje neurons," *J. Neurosci.*, vol. 17, no. 12, pp. 4517–4526, Jun. 1997.

[36] W. A. Kues and F. Wunder, "Heterogeneous expression patterns of mammalian potassium channel genes in developing and adult rat brain," *Eur. J. Neurosci.*, vol. 4, no. 12, pp. 1296–1308, Dec. 1992.

[37] R. W. Veh, R. Lichtinghagen, S. Sewing, F. Wunder, I. M. Grumbach, and O. Pongs, "Immunohistochemical localization of five members of the KV1 channel subunits: Contrasting subcellular locations and neuron-specific co-localizations in rat brain," *Eur. J. Neurosci.*, vol. 7, no. 11, pp. 2189–2205, Nov. 1995.

[38] A. Lorincz and Z. Nusser, "Molecular identity of dendritic voltage-gated sodium channels," *Science*, vol. 328, no. 5980, pp. 906–909, May 2010.

[39] E. Benoit and J. M. Dubois, "Properties of maintained sodium current induced by a toxin from androctonus scorpion in frog node of Ranvier," *J. Physiol.*, vol. 383, no. 1, pp. 93–114, Feb. 1987.

[40] J. M. Dubois and C. Bergman, "Late sodium current in the node of Ranvier," *Pflügers Arch. Eur. J. Physiol.*, vol. 357, nos. 1–2, pp. 145–148, 1975.

[41] M. Stefano, F. Cordella, and L. Zollo, "Intraneural electrical stimulation of median nerve: A simulation study on sensory and motor fascicles," *J. Biol. Regulators Homeost Agents*, vol. 34, no. 5, pp. 127–136, 2020.

[42] M. Stefano, F. Cordella, and L. Zollo, "The intraneural electrical stimulation of human median nerve: A simulation study," in *Proc. 29th IEEE Int. Conf. Robot Hum. Interact. Commun. (RO-MAN)*, Aug./Sep. 2020, pp. 671–676.

[43] R. Fitzhugh, "Computation of impulse initiation and saltatory conduction in a myelinated nerve fiber," *Biophys. J.*, vol. 2, no. 1, pp. 11–21, Jan. 1962.

[44] L. Goldman and J. S. Albus, "Computation of impulse conduction in myelinated fibers; theoretical basis of the velocity-diameter relation," *Biophys. J.*, vol. 8, no. 5, pp. 596–607, May 1968.

[45] D. R. McNeal, "Analysis of a model for excitation of myelinated nerve," *IEEE Trans. Biomed. Eng.*, vol. BME-23, no. 4, pp. 329–337, Jul. 1976.

[46] J. D. Sweeney, J. T. Mortimer, and D. Durand, "Modeling of mammalian myelinated nerve for functional neuromuscular stimulation," in *Proc. IEEE EMBC Annu. Conf.*, 1997, pp. 1577–1578.

[47] J. W. Moore, R. W. Joyner, M. H. Brill, S. D. Waxman, and M. Najar-Joa, "Simulations of conduction in uniform myelinated fibers. Relative sensitivity to changes in nodal and internodal parameters," *Biophys. J.*, vol. 21, no. 2, pp. 147–160, Feb. 1978.

[48] J. Patlak, "Molecular kinetics of voltage-dependent Na^+ channels," *Physiol. Rev.*, vol. 71, no. 4, pp. 1047–1080, Oct. 1991.

[49] J. X. Zhou, X. Qiu, A. F. d'Hérouël, and S. Huang, "Discrete gene network models for understanding multicellularity and cell reprogramming: From network structure to attractor landscape," in *Computational Systems Biology*, 2nd ed. Amsterdam, The Netherlands: Elsevier, 2014, pp. 241–276.

[50] E. Vigmond and G. Plank, *Cardiac Modeling*. Amsterdam, The Netherlands: Elsevier, 2019, pp. 1–20.

[51] C. C. McIntyre and W. M. Grill, "Sensitivity analysis of a model of mammalian neural membrane," *Biol. Cybern.*, vol. 79, no. 1, pp. 29–37, Aug. 1998.

[52] A. L. Hodgkin and A. F. Huxley, "A quantitative description of membrane current and its application to conduction and excitation in nerve," *J. Physiol.*, vol. 117, no. 4, pp. 500–544, 1952.

[53] M. Pospischil *et al.*, "Minimal Hodgkin–Huxley type models for different classes of cortical and thalamic neurons," *Biol. Cybern.*, vol. 99, nos. 4–5, pp. 427–441, Nov. 2008.

[54] P. Balbi, P. Massobrio, and J. H. Kotaleski, "A single Markov-type kinetic model accounting for the macroscopic currents of all human voltage-gated sodium channel isoforms," *PLoS Comput. Biol.*, vol. 13, no. 9, Sep. 2017, Art. no. e1005737.

[55] B. Feng, Y. Zhu, J.-H. La, Z. P. Wills, and G. F. Gebhart, "Experimental and computational evidence for an essential role of $Na_V1.6$ in spike initiation at stretch-sensitive colorectal afferent endings," *J. Neurophysiol.*, vol. 113, no. 7, pp. 2618–2634, Apr. 2015.

[56] C. Peters, R. E. Rosch, E. Hughes, and P. C. Ruben, "Temperature-dependent changes in neuronal dynamics in a patient with an SCN1A mutation and hyperthermia induced seizures," *Sci. Rep.*, vol. 6, no. 1, p. 31879, Oct. 2016.

[57] M. Ye *et al.*, "Differential roles of $Na_V1.2$ and $Na_V1.6$ in regulating neuronal excitability at febrile temperature and distinct contributions to febrile seizures," *Sci. Rep.*, vol. 8, no. 1, p. 753, Dec. 2018.

[58] R. Ranjan *et al.*, "A kinetic map of the homomeric voltage-gated potassium channel (Kv) family," *Frontiers Cellular Neurosci.*, vol. 13, p. 358, Aug. 2019.

[59] R. Ranjan *et al.*, "Channelpedia: An integrative and interactive database for ion channels," *Frontiers Neuroinformat.*, vol. 5, p. 36, Dec. 2011.

[60] D. K. Sharma and A. R. Garg, "Dynamics of HH model for excitable neuron with added voltage gated calcium channel," in *Proc. Nat. Conf. Adv. Technol. Appl. Sci.*, 2014, vol. 975, no. 2, p. 8887.

[61] G. M. Faber, J. Silva, L. Livshitz, and Y. Rudy, "Kinetic properties of the cardiac L-type Ca^{2+} channel and its role in myocyte electrophysiology: A theoretical investigation," *Biophysical J.*, vol. 92, no. 5, pp. 1522–1543, Mar. 2007.

[62] A. E. Alekseev, N. I. Markevich, A. F. Korystova, A. Terzic, and Y. M. Kokoz, "Comparative analysis of the kinetic characteristics of L-type calcium channels in cardiac cells of hibernators," *Biophysical J.*, vol. 70, pp. 786–797, Feb. 1996.

[63] B. Frankenhauser and A. F. Huxley, "The action potential in the myelinated nerve fibre of Xenopus laevis as computed on the basis of voltage clamp data," *J. Physiol.*, vol. 171, no. 2, pp. 302–315, 1964.

[64] J. P. Reilly, V. T. Freeman, and W. D. Larkin, "Sensory effects of transient electrical stimulation–evaluation with a neuroelectric model," *IEEE Trans. Biomed. Eng.*, vol. BME-32, no. 12, pp. 1001–1011, Dec. 1985.

[65] P. H. Gorman and J. T. Mortimer, "The effect of stimulus parameters on the recruitment characteristics of direct nerve stimulation," *IEEE Trans. Biomed. Eng.*, vol. BME-30, no. 7, pp. 407–414, Jul. 1983.

[66] J. H. Meier, W. L. C. Rotten, A. E. Zoutman, H. B. K. Boom, and P. Bergveld, "Simulation of multipolar fiber selective neural stimulation using intrafascicular electrodes," *IEEE Trans. Biomed. Eng.*, vol. 39, no. 2, pp. 122–134, Feb. 1992.

[67] J. H. M. Frijns and J. H. T. Kate, "A model of myelinated nerve fibres for electrical prosthesis design," *Med. Biol. Eng. Comput.*, vol. 32, no. 4, pp. 391–398, Jul. 1994.

[68] G. M. Schoepfle and J. Erlanger, "The action of temperature on the excitability, spike height and configuration, and the refractory period observed in the responses of single medullated nerve fibers," *Amer. J. Physiol.-Legacy Content*, vol. 134, no. 4, pp. 694–704, Oct. 1941.

[69] E. F. Barrett and J. N. Barrett, "Intracellular recording from vertebrate myelinated axons: Mechanism of the depolarizing afterpotential," *J. Physiol.*, vol. 323, no. 1, pp. 117–144, Feb. 1982.

[70] A. R. Blight and S. Someya, "Depolarizing afterpotentials in myelinated axons of mammalian spinal cord," *Neuroscience*, vol. 15, no. 1, pp. 1–12, May 1985.

[71] A. R. Blight, "Computer simulation of action potentials and afterpotentials in mammalian myelinated axons: The case for a lower resistance myelin sheath," *Neuroscience*, vol. 15, no. 1, pp. 13–31, May 1985.

[72] F. Awiszus, "Effects of paranodal potassium permeability on repetitive activity of mammalian myelinated nerve fiber models," *Biol. Cybern.*, vol. 64, no. 1, pp. 66–76, 1990.

[73] J. A. Halter and J. W. Clark, "A distributed-parameter model of the myelinated nerve fiber," *J. Theor. Biol.*, vol. 148, no. 3, pp. 345–382, Feb. 1991.

[74] H. Bostock, M. Baker, and G. Reid, "Changes in excitability of human motor axons underlying post-ischaemic fasciculations: Evidence for two stable states," *J. Physiol.*, vol. 441, no. 1, pp. 537–557, Sep. 1991.

[75] D. I. Stephanova and H. Bostock, "A distributed-parameter model of the myelinated human motor nerve fibre: Temporal and spatial distributions of action potentials and ionic currents," *Biol. Cybern.*, vol. 73, no. 3, pp. 275–280, Aug. 1995.

[76] A. G. Richardson, C. C. McIntyre, and W. M. Grill, "Modelling the effects of electric fields on nerve fibres: Influence of the myelin sheath," *Med. Biol. Eng. Comput.*, vol. 38, no. 4, pp. 438–446, Jul. 2000.

[77] C. C. McIntyre, A. G. Richardson, and W. M. Grill, "Modeling the excitability of mammalian nerve fibers: Influence of afterpotentials on the recovery cycle," *J. Neurophysiol.*, vol. 87, no. 2, pp. 995–1006, Feb. 2002.

[78] J. R. Schwarz, G. Reid, and H. Bostock, "Action potentials and membrane currents in the human node of Ranvier," *Pflügers Archiv Eur. J. Physiol.*, vol. 430, no. 2, pp. 283–292, Jun. 1995.

[79] B. V. Safronov, K. Kampe, and W. Vogel, "Single voltage-dependent potassium channels in rat peripheral nerve membrane," *J. Physiol.*, vol. 460, no. 1, pp. 675–691, Jan. 1993.

[80] K. Zhu, L. Li, X. Wei, and X. Sui, "A 3D computational model of transcutaneous electrical nerve stimulation for estimating Aß tactile nerve fiber excitability," *Frontiers Neurosci.*, vol. 11, p. 250, May 2017.

[81] C. W. Elder and P. B. Yoo, "A finite element modeling study of peripheral nerve recruitment by percutaneous tibial nerve stimulation in the human lower leg," *Med. Eng. Phys.*, vol. 53, pp. 32–38, Mar. 2018.

[82] A. Kuhn, T. Keller, M. Lawrence, and M. Morari, "A model for transcutaneous current stimulation: Simulations and experiments," *Med. Biol. Eng. Comput.*, vol. 47, no. 3, pp. 279–289, Mar. 2009.

[83] M. A. Schiefer, R. J. Triolo, and D. J. Tyler, "A model of selective activation of the femoral nerve with a flat interface nerve electrode for a lower extremity neuroprosthesis," *IEEE Trans. Neural Syst. Rehabil. Eng.*, vol. 16, no. 2, pp. 195–204, Apr. 2008.

[84] P. Schier *et al.*, "Model-based vestibular afferent stimulation: Evaluating selective electrode locations and stimulation waveform shapes," *Frontiers Neurosci.*, vol. 12, p. 588, Aug. 2018.

[85] A. Q. Choi, J. K. Cavanaugh, and D. M. Durand, "Selectivity of multiple-contact nerve cuff electrodes: A simulation analysis," *IEEE Trans. Biomed. Eng.*, vol. 48, no. 2, pp. 165–172, Feb. 2001.

[86] C. A. Bossetti, M. J. Birdno, and W. M. Grill, "Analysis of the quasi-static approximation for calculating potentials generated by neural stimulation," *J. Neural Eng.*, vol. 5, no. 1, pp. 44–53, Mar. 2008.

[87] F. Kolbl, M. C. Juan, and F. Sepulveda, "Impact of the angle of implantation of transverse intrafascicular multichannel electrodes on axon activation," in *Proc. IEEE Biomed. Circuits Syst. Conf. (BioCAS)*, Oct. 2016, pp. 484–487.

[88] J. Perez-Perive and D. M. Durund, "Modeling study of peripheral nerve recording selectivity," *IEEE Trans. Rehabil. Eng.*, vol. 8, no. 3, pp. 320–329, Sep. 2000.

[89] C. H. Lubba *et al.*, "PyPNS: Multiscale simulation of a peripheral nerve in Python," *Neuroinformatics*, vol. 17, no. 1, pp. 63–81, Jan. 2019.

[90] A. K. Ramrakhyani, Z. B. Kagan, D. J. Warren, R. A. Normann, and G. Lazzi, "A μm-scale computational model of magnetic neural stimulation in multifascicular peripheral nerves," *IEEE Trans. Biomed. Eng.*, vol. 62, no. 12, pp. 2837–2849, Dec. 2015.